Solution Structure of the Coxsackievirus and Adenovirus Receptor Domain 1[†,‡]

Shaokai Jiang,[⊥] Amy Jacobs,[⊥] Thomas M. Laue,[§] and Michael Caffrey*[,⊥]

Department of Biochemistry and Moleular Genetics, University of Illinois at Chicago, Chicago, Illinois 60607, and Center to Advance Molecular Interaction Science, University of New Hampshire, Durham, New Hampshire 03824

Received August 20, 2003; Revised Manuscript Received December 11, 2003

ABSTRACT: The coxsackievirus and adenovirus receptor (CAR) mediates entry of coxsackievirus B (CVB) and adenovirus (Ad). The normal cellular function of CAR, which is expressed in a wide variety of tissue types, is thought to involve homophilic cell adhesion in the developing brain. The extracellular domain of CAR consists of two immunoglobulin (Ig) domains termed CAR-D1 and CAR-D2. CAR-D1 is shown by sedimentation velocity to be monomeric at pH 3.0. The solution structure and the dynamic properties of monomeric CAR-D1 have been determined by NMR spectroscopy at pH 3.0. The determinants of the CAR-D1 monomer−dimer equilibrium, as well as the binding site of CVB and Ad on CAR, are discussed in light of the monomer structure.

It is estimated that ∼5% of the world's population is currently infected with the coxsackievirus B, CVB[1] (*1*). The presence of CVB is widespread, and the occurrence of small epidemics is well documented. Children and individuals with a suppressed immune system are especially sensitive to CVB infection (*2*). CVB is a major cause of viral heart infections (acute myocarditis and pericarditis), which lead to over 9000 deaths annually in the United States (*3*−*5*). Moreover, CVB infection has been implicated in many other diseases including aseptic meningitis, fetal demise, and diabetes mellitus (*6*). At present, there are no effective therapies against CVB infection and the resulting deleterious health effects. Consequently, a vaccine or antiviral drug for the treatment of CVB infection is highly desirable.

CVB infection requires attachment of the virus to the target membrane and subsequent entry of the virus into the target cytoplasm. It has been shown that the coxsackievirus and adenovirus receptor (CAR) mediates viral attachment and entry, and thus it is established as the CVB receptor (*7*−*9*). Note, however, that other CVB receptors may play roles in attachment and postattachment events of the viral life cycle (*10*). Interestingly, CAR has been shown to be the receptor for both CVB and adenovirus (Ad), even though CVB and Ad evolved separately and do not share the same host range. The normal cellular function of CAR is thought to involve homophilic cell adhesion in the developing brain (*11*). The gene for CAR codes for a protein of ∼365 amino acids, which is bound to the outer membrane of many tissue types including those from the heart, a target site for CVB infection. CAR consists of two extracellular immunoglobulin (Ig) domains (CAR-D1/D2) followed by transmembrane (TM) and intracellular domains. CAR-D1/D2, which consists of ∼235 amino acids, has been shown to possess all of the necessary characteristics for CVB attachment and entry when anchored to the membrane by glycosylphophatidylinositol, GPI (*12*). Moreover, CAR lacking the cytoplasmic domain (tailless CAR) has been shown to support Ad infection (*13*). Consequently, the TM and cytoplasmic domains are not critical to CVB (and presumably Ad) infection.

Previously, the crystal structures of CAR-D1 as a dimer and CAR-D1 bound to the Ad fiber head have been obtained (*14*, *15*). Moreover, the complex between CAR-D1/D2 and CVB has been visualized by cryoelectron microscopy at 22 Å resolution (*16*). As part of our desire to use NMR for the discovery of novel therapies against chronic CVB infection (and possibly Ad infection), we have initiated study of CAR-D1 by NMR spectroscopy (*17*). In the present work, we have characterized the solution structure and dynamic properties of monomeric CAR-D1, which is the predominant form in vivo.

EXPERIMENTAL PROCEDURES

Sedimentation Velocity Studies. The preparation of human CAR-D1 (residues 21−144) is described elsewhere (*17*). Sedimentation velocity studies were carried out in a Beckman model XL-A analytical ultracentrifuge using absorbance optics at 280 nm. Runs were performed at a protein concentration range of 0.619 mg/mL at 60 000 rpm and 20 °C. The sedimentation coefficient distribution was calculated by time derivative analysis using a single species fit of the data of 30 averaged scans (*18*) using the program DCDT+ (*19*). The buffer conditions were 50 mM sodium formate at pH 3 with a buffer density of 0.998 94 g/cm^3. At pH 3, the charge of CAR-D1 is estimated to be +16.4. Based on the amino acid sequence, the partial specific volume was estimated to be 0.7430 cm^3/g. The derived sedimentation and diffusion coefficients were 1.464 ± 0.001 S and 9.98 ± 0.03 Ficks, respectively.

[†] This work was supported by an American Heart Association Scientist Development Grant to M.C. and Grants NIH 5R01GM062836 and NSF DBI 987652 to T.L.

[‡] The coordinates of the minimized mean structure and 30 low-energy structures of CAR-D1 have been deposited in the Protein Data Bank (ID = 1RSF). The relaxation data have been deposited in the BioMagResBank (BMRB-8987).

* To whom correspondence should be addressed.

[⊥] University of Illinois at Chicago.

[§] University of New Hampshire.

[1] Abbreviations: Ad, adenovirus; CAR, coxsackievirus and adenovirus receptor; CAR-D1, CAR domain 1; CVB, coxsackievirus B.

10.1021/bi035490x CCC: $27.50
Published on Web 01/30/2004

Structure Calculations. NMR experiments and assignments have been described previously (*17*). An additional HNHA experiment was performed to add $^3J_{HN\alpha}$ information. The CAR-D1 structure was calculated by the program CNS (*20*) using the protocol described by Guilhaudis et al. (*21*). For the homonuclear, ^{13}C-edited and ^{15}N-edited NOESY experiments, the mixing times ranged from 100 to 150 ms. Initial structures were calculated by a torsion angle dynamics protocol starting from an extended strand structure followed by conventional simulated annealing in Cartesian space. The experimental restraints included 1265 NOEs, 230 dihedral angles (based on ^3J bond couplings and analysis of backbone chemical shifts by the program TALOS (*22*)), and 56 H bonds (based on a H_N exchange experiment in D_2O). The electrostatic map and structural figures were generated by the molecular graphics program MOLMOL (*23*).

Characterization of Dynamics. The ^{15}N R_z ($1/T_1$), R_{xy} ($1/T_2$), and HNOE values were measured by standard pulse sequences (reviewed in ref *24*). A total of seven data sets were collected to measure R_z with delay values of 11.8, 31.8, 61.8, 121.8, 241.8, 481.8, and 721.8 ms; a total of seven data sets were collected to measure R_{xy} with delay values of 8, 16, 32, 64, 128, 192, and 256 ms. The decays of cross-peak intensities with time in the ^{15}N R_z and R_{xy} experiments were fit to a single exponential by a nonlinear least-squares fit with fitting errors typically less than 5% (Kaleidagraph 3.08, Synergy Software). HNOE values for each given residue were calculated as the volume ratio (V/V_0) of the ^{15}N−^{1}H correlation peak in the presence (V) and absence (V_0) of proton saturation during the relaxation delay of 5 s. Errors in the HNOE were estimated by the method of Nicholson et al. (*25*). Accordingly, the average error in the HNOE was estimated to be ±0.04. Analysis of rotational diffusion and internal mobility was performed by the program Tensor version 2.0 (*26*). Based on R_{xy}/R_z ratios and a Monte Carlo error analysis, the isotropic model was determined to be the most appropriate diffusion model. The isotropic model for rotational diffusion was then used in a Lipari−Szabo-type analysis of the internal mobility (*27*).

RESULTS

Hydrodynamic Properties of CAR-D1. Previous studies by analytical ultracentrifugation have shown that CAR-D1 is in a monomer−dimer equilibrium at neutral pH ($K_d \approx 16$ μM, *14*). Initial NMR experiments on CAR-D1 were performed at pH 6.0. On the basis of the average H_N T_2 of ∼16 ms, CAR-D1 is predominantly a dimer at pH 6.0 and has a concentration of >300 μM, an observation that is consistent with the analytical ultracentrifugation studies. Subsequently, it was observed that CAR-D1 samples prepared in 50 mM formate, pH 3.0, exhibited good spectral dispersion and a significantly increased average H_N T_2 (∼29 ms) at 1 mM concentration, suggesting that at low pH CAR-D1 is folded and monomeric under these solution conditions. Consequently, sedimentation velocity experiments (reviewed in ref *28*) were performed to better characterize the hydrodynamic properties of CAR-D1 at pH 3.0. As shown in Figure 1, the sedimentation coefficient of CAR-D1 is ∼1.5 at pH 3.0, and thus the data fit to a molecular weight of 14.1 kDa (cf. Experimental Procedures). Based on the amino acid sequence of CAR-D1 and MALDI-TOF mass spectrometry, the molecular weight of CAR-D1 is 14.0 kDa, and thus the sedimentation velocity results demonstrate that the CARD1 is completely monomeric under the conditions of the sedimentation experiment. Even a small (1−2%) quantity of dimer would have been apparent in these experiments. Hence, even if there were a weak association to dimer under these conditions, the maximum amount of dimer present at the concentration used in the NMR experiments would be <5% on a molar basis.

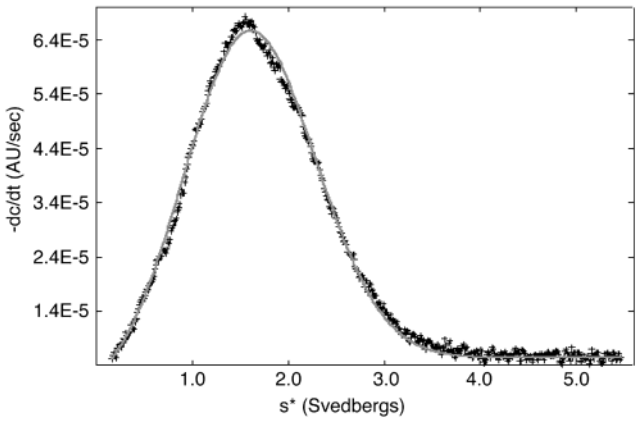

FIGURE 1: Sedimentation velocity experiment of CAR-D1 at pH 3.0. The light gray line corresponds to a fit of the data to a single species (cf. Experimental Procedures). Experimental conditions were 45 μM CAR-D1 (0.62 mg/mL) in 50 mM sodium formate, pH 3.0, at 20 °C.

Solution Structure of CAR-D1. The native state of CAR-D1 is monomeric (to be discussed below), and thus, we have determined the solution structure of CAR-D1 at pH 3.0, a condition where CAR-D1 is folded and monomeric. The solution structure of CAR-D1 was determined by standard NMR methods using information from NOEs, H-bonds, ^3J coupling constants, and chemical shifts (summarized in Table 1). Attempts to align CAR-D1 at low pH in the presence of poly(ethylene glycol)/hexanol (cf. *30*) were not productive due to an interaction between CAR-D1 and the alignment media. Thus, the present structure was determined without structural information from residual dipolar couplings. The resulting ensemble of low-energy structures and the minimized mean structure of monomeric CAR-D1 are shown in Figure 2. The structural statistics of the final ensemble and the minimized mean are summarized in Table 1. The N- and C-termini of CAR-D1 (residues 19−21 and 139−144, respectively) are not in a regular secondary structure and exhibit higher root-mean-square deviation (RMSD) values (Figure 2a), suggesting that they are not well ordered in solution. For the ensemble of 30 low-energy structures, the RMSD of residues 26−138 to the mean is 0.39 and 0.86 Å for the backbone and heavy atoms, respectively (Figure 2a, Table 1). The RMSD of residues in β sheet structures is 0.28 and 0.71 Å for the backbone and heavy atoms, respectively (Figure 2a, Table 1). As shown in Figure 2b, the overall folding motif of CAR-D1 consists of antiparallel β sheets in a V-type Ig domain fold. In the context of the native CAR, CAR-D1 is followed in sequence by CAR-D2 and a transmembrane domain (*7*−*9*); thus, the direction of the cellular membrane can be deduced from the location of the CAR-D1 C-terminus (Figure 2b). As shown in Figure 2b, the 2 layers of β-sheets are connected by a disulfide bond between cysteines 41 and 120. We note that we were unable to successfully refold a CAR-D1 mutant in which cysteines

Table 1: Structural Statistics[a]

	⟨SA⟩	⟨SA⟩$_r$
RMS Deviations from Distance Restraints		
all (1265)	0.035 ± 0.003	0.036
intraresidue (316)	0.030 ± 0.009	0.028
sequential ($\|i-j\|=1$) (343)	0.044 ± 0.007	0.043
short range ($1<\|i-j\|<5$) (132)	0.034 ± 0.012	0.039
long range ($\|i-j\|>5$) (474)	0.029 ± 0.006	0.037
RMS deviations from dihedral restraints (deg) (230)[b]	1.46 ± 0.04	0.85
Deviations from Idealized Covalent Geometry		
bonds (Å)	0.005 ± 0.001	0.007
angles (deg)	0.63 ± 0.03	0.66
impropers (deg)	0.57 ± 0.04	0.59
Measures of Structure Quality[c]		
% residues in most favorable regions	83.8 ± 4.2	82.4
% residues in additionally allowed regions	16.0 ± 3.4	17.6
% residues in generously allowed regions	0.2 ± 0.0	0.0
% residues in disallowed regions	0.0 ± 0.0	0.0
number of bad contacts/100 residues	6.0 ± 6.0	8.0
Coordinate Precision[d]		
backbone residues 26−138 (Å)	0.39 ± 0.06	
heavy residues 26−138 (Å)	0.86 ± 0.06	
β sheet backbone (Å)	0.28 ± 0.04	
β sheet heavy (Å)	0.71 ± 0.06	

[a] Structural statistics for the final 30 simulated annealing structures (⟨SA⟩) and the minimized mean structure (⟨SA⟩$_r$). None of the structures exhibited distance violations greater than 0.5 Å or dihedral violations greater than 5°. [b] Torsion angle restraints consisted of 115 ϕ and 115 ψ. [c] The overall quality of the structure was assessed by the program PROCHECK 3.5 (*29*). [d] Defined as average RMS difference between the final 30 simulated annealing structures and the mean coordinates.

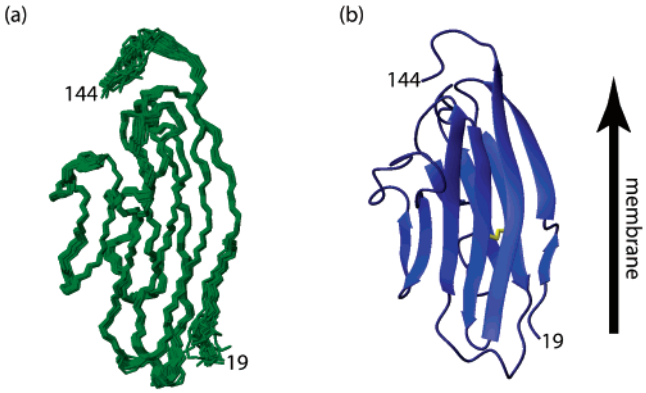

FIGURE 2: Solution structure of the CAR-D1 monomer at pH 3.0: (a) ensemble of 30 low-energy CAR-D1 structures; (b) ribbon diagram of CAR-D1 minimized mean structure. The disulfide bond between cysteines 41 and 120 is depicted in yellow. The direction of the C-terminus of CAR-D1 and hence D2 and the membrane in native CAR is shown by an arrow.

41 and 120 were substituted by alanines, an observation that suggests that the cysteine pair is critical to the CAR-D1 folding pathway, stability of the native state, or both. Interestingly, several observations indicate that P126 is in the cis conformation. First, the H_α of A125 exhibits a strong NOE to the H_α of P126 and a very weak NOE to the H_δ of P126. Second, the chemical shift of the P126 C_β is shifted upfield with respect to random coil values, an observation that is consistent with the chemical shifts observed for the cis conformation of proline (*31*). On the basis of ^{13}C chemical shifts and NOE patterns, all other prolines are in the trans conformation. In Figure 3a, the locations of the hydrophobic side chains are depicted in green. The majority of the hydrophobic side chains are located in the protein interior and thus serve to stabilize the interaction of the two layers of β sheets. In contrast, there are nine hydrophobic side chains that are highly exposed. Exposed hydrophobic side chains are often involved in protein−protein interactions (*32*, *33*), and since CAR-D1 is known to interact with numerous protein surfaces, the locations of the exposed hydrophobic side chains may be of special interest. As shown in Figure 3a, the exposed hydrophobic side chains of the CAR-D1 monomer fall into two regions: "front side" (L58, V67, L70, L73, and V128) and "top" (L112, V136, L138, and V139). As will be discussed below, the "front side" hydrophobics occur in the proximity of the CAR-D1 protein−protein interaction site. The "top" hydrophobic side chains are located at the C-terminus of CAR-D1, and thus it is reasonable to hypothesize that they may form direct interactions with the D2, which immediately follows D1. The electrostatic potential of CAR-D1 at neutral pH is shown in Figure 3b. In general, the CAR-D1 surface consists of alternating stripes of basic and acidic patches that are uniformly distributed. The special significance of three charged groups (D54, E56, and K123), which are in close proximity to one group of the exposed hydrophobic side chains (L58, V67, L70, L73, and V128), will be discussed below. Finally, we note that the side chain of N106, which is the sole glycosylation site of CAR-D1 (*16*), is well exposed in the solution structure (data not shown).

Dynamic Properties of CAR-D1. The dynamic properties of monomeric CAR-D1 were characterized by determination of heteronuclear relaxation rates, which have been widely used to investigate the backbone dynamics of proteins and the role of dynamics in protein function (reviewed in refs *34* and *35*). The ^{15}N R_z and R_{xy} relaxation rates and the $^1H-^{15}N$ NOE (HNOE) were determined for each residue in CAR-D1 (Figure 4a−c). The average R_z, R_{xy}, and the HNOE values of the CAR-D1 core (residues 28−139) are 1.28 s^{-1}, 10.6 s^{-1}, and 0.56, respectively. Residues 19−21 and 140−144, which are located at the N- and C-termini and not part of a regular secondary structure, exhibit relaxation parameters that suggest a less-ordered structure. The uniformity of the relaxation parameters suggests that CAR-D1 is relatively rigid. To better interpret the dynamic properties of CAR-D1, the three relaxation parameters were analyzed by the program Tensor (*26*), which determines the appropriate rotational diffusion model and fits the data to a model-free analysis of internal mobility. Based on the R_{xy}/R_z values, the isotropic rotational diffusion tensor was deemed to be the most appropriate hydrodynamic model, a conclusion that is consistent with the overall shape of the CAR-D1 monomer (cf. Figure 3b). The resulting correlation time was determined to be 8.64 ± 0.07 ns, a value that indicates that CAR-D1 is indeed monomeric at pH 3.0. The derived S^2 values, which reflect the relative mobility of the protein backbone, are shown in Figure 4d, and their placement in the CAR-D1 structure is shown in Figure 4e. As expected from the uniform R_z, R_{xy}, and HNOE values of the CAR-D1 core, the derived S^2 values are also relatively uniform with an average value of 0.76. The N- and C-termini of CAR-D1 (residues

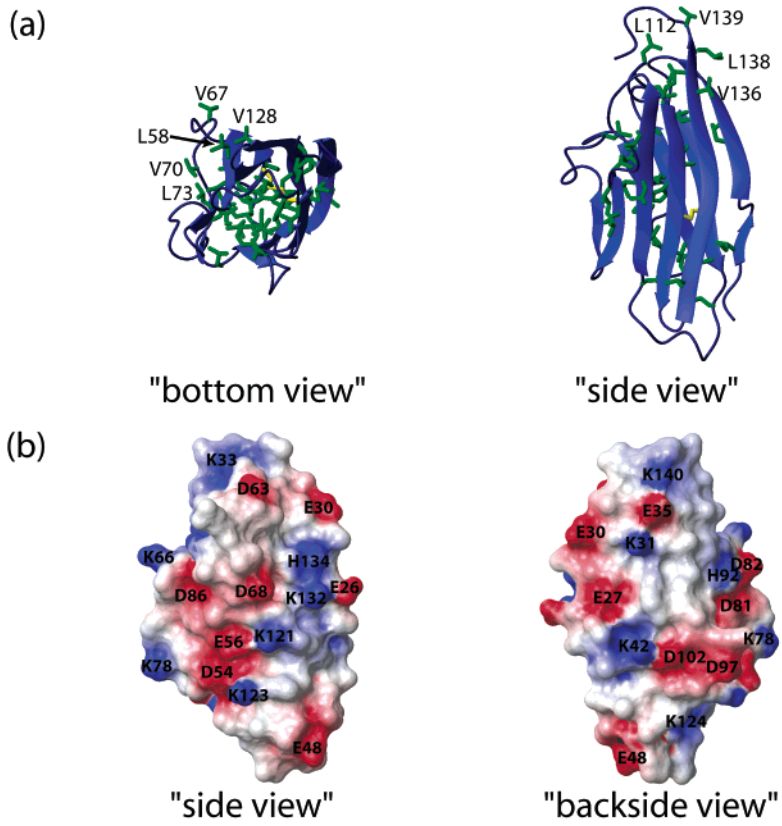

FIGURE 3: Structural features of the CAR-D1 monomer: (a) two views of the hydrophobic side chains (V, L, I, F, and W) are shown in green; the exposed hydrophobic side chains are labeled; (b) two views of the electrostatic map with the exposed charged side chains labeled.

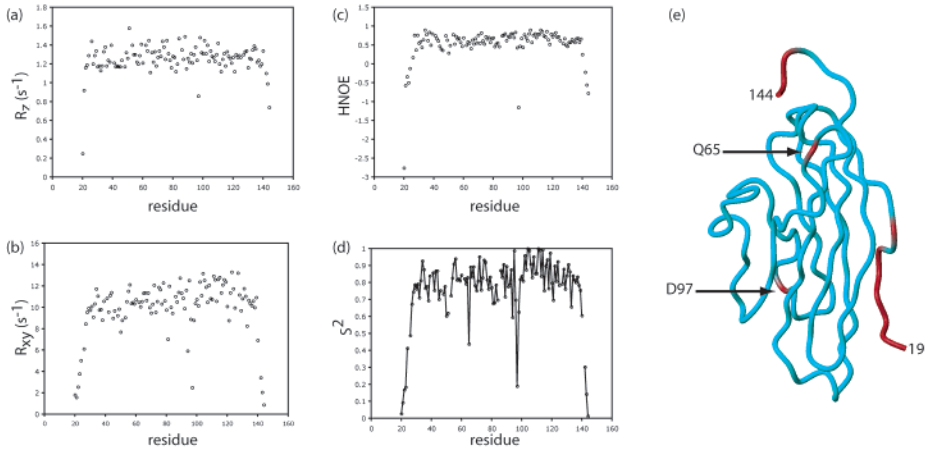

FIGURE 4: Dynamic properties of monomeric CAR-D1: relaxation parameters (a) ^{15}N R_z, (b) ^{15}N R_{xy}, and (c) HNOE, and (d) the derived order parameter (S^2). For the determination of S^2, an isotropic model of diffusion was employed with a correlation time of 8.64 ns. Experimental conditions were 1 mM CAR-D1 and 50 sodium formate, pH 3.0, at 22 °C. Panel e shows correlation of S^2 with the backbone structure of the CAR-D1 monomer. Cyan regions represent the highest S^2 values; red regions represent the lowest S^2 values.

20−27 and 140−144) exhibit lower S^2 values suggesting more mobility, and many require the additional terms internal correlation time (τ_e) and a second-order parameter (Sf^2) to fit the relaxation parameters. The relative mobility of the N- and C-termini suggested by the decreased S^2 values is consistent with their larger average backbone RMSD (Figure 2a). Interestingly, residues 65 and 97 exhibit $S^2 < 0.60$, which is significantly lower than the other core residues. These residues are located in loop regions and are apparently more mobile than the other residues of the CAR-D1 core. Residues 20, 78, 82, 89, 91, 115, 118, 123, 127, and 139 require a R_{ex} term to include conformational exchange on the microsecond to millisecond time scale, although the significance of this observation is unknown at present. In summary, the dynamic properties of CAR-D1 at pH 3.0 suggest that it is monomeric under these conditions and that the protein as a whole behaves as a relatively rigid sphere.

DISCUSSION

Comparison of the Monomeric, Dimeric, and Adenovirus-Bound States of CAR-D1. The present work represents the first structure of CAR-D1 in the monomeric state. As discussed above, the structure of the CAR-D1 dimer has been determined by X-ray crystallography at pH 5.2 (*14*). Con-

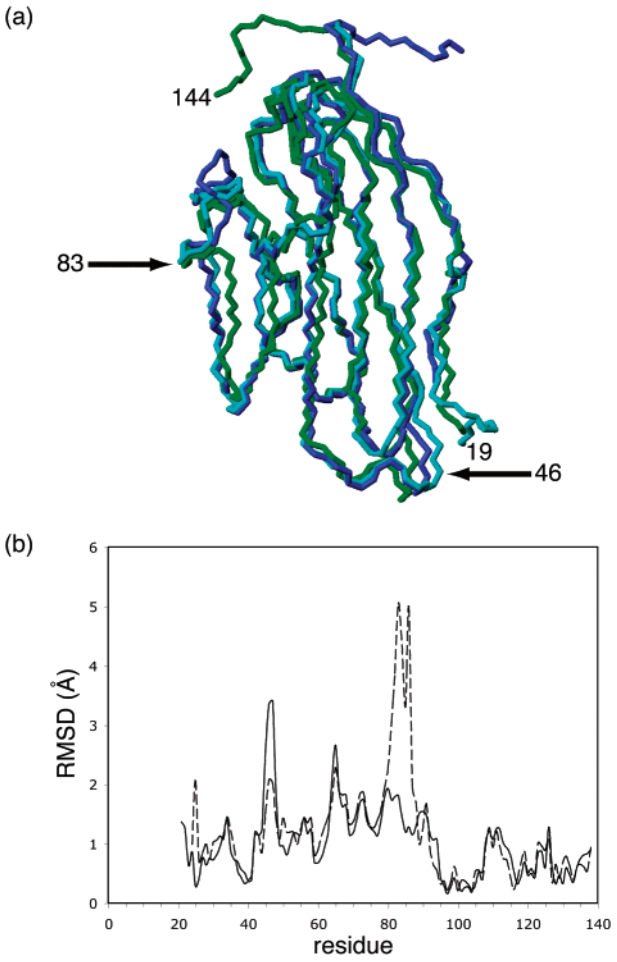

FIGURE 5: Overlay of CAR-D1 structures (a) determined by NMR (green) and X-ray (blue and cyan). The structure of CAR-D1 found as one subunit of a homodimer (*14*) is shown in cyan. The structure of CAR-D1 found in the complex with the Ad fiber head (*15*) is shown in blue. Panel b shows the average backbone RMSD of monomeric CAR-D1 to one subunit of the dimer (solid line) and the Ad-bound monomer (dashed line).

sequently, it is of interest to compare the low-pH monomer structure of CAR-D1 to the dimeric form. As shown in Figure 5a by a comparison of the monomer (green) and one subunit of the dimer (cyan), the CAR-D1 structures are very similar with an average backbone RMSD of 1.2 Å for residues 22−138, which suggests that the CAR-D1 backbone structure does not change as a function of pH. The largest differences between the monomer and dimer backbone structures occur for three residues in the vicinity of S46 (residues 45−47, Figure 5a,b), which are located in a loop region and exhibit average backbone RMSD of ∼3.4 Å. The structure of the CAR-D1 monomer bound to the Ad fiber head has also been determined by X-ray crystallography (*15*). As shown in Figure 5a by a comparison of the monomer (green) and Ad-bound (blue) CAR-D1 structures, the structures are again very similar with an average backbone RMSD of 1.5 Å for residues 22−138, which suggests that the CAR-D1 backbone structure does not change significantly upon binding to Ad. The largest differences between the monomer and Ad-bound backbone structures occur for seven residues in the vicinity of Y83 (residues 80−86, Figure 5a,b), which are located in a loop region and exhibit average backbone RMSD of ∼3.8 Å. Finally, for reference it is important to note that the

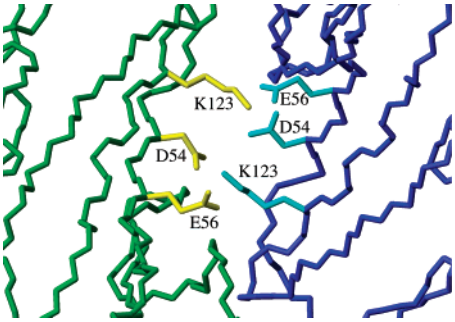

FIGURE 6: Electrostatic contacts observed in the CAR-D1 dimer at pH 5.2. The subunits of CAR-D1 are colored green and blue. Coordinates were taken from the X-ray structure of the CAR-D1 dimer (*14*).

average backbone RMSD between the dimer and Ad-bound structures, both determined by X-ray crystallography (*14*, *15*), is 0.9 Å for residues 22−138.

Determinants of the CAR-D1 Monomer−Dimer Equilibrium. It is next of interest to examine the determinants of the CAR-D1 monomer−dimer equilibrium. As discussed above, at low pH CAR-D1 is monomeric (data presented herein), and at neutral pH, CAR-D1 is in equilibrium between monomeric and dimeric states with a $K_d \approx 16\ \mu M$ (*14*). The X-ray structure, which was determined at pH 5.2, represents the dimeric state of CAR-D1. As shown in Figure 6, examination of the X-ray structure of the CAR-D1 dimer shows that D54 and E56 of one subunit form apparent electrostatic interactions with K123 of the other subunit. For example, the D54 Oδ1−K123 Nζ average distance is ∼3.1 Å, and the E56 Oϵ2−K123 Nζ average distance is 3.1 Å in the CAR-D1 dimer, which is within the 4 Å distance typically observed for ion pairs in proteins (*36*). At pH 3.0, the side chains of D54 and E56 are expected to be protonated, and thus their intersubunit electrostatic interactions with K123 are expected to be absent. The results presented herein demonstrate that CAR-D1 is monomeric at pH 3.0, and thus, it is reasonable to posit that intersubunit electrostatic interactions among these three residues (D54, E56, and K123) are the determining factor in the CAR-D1 monomer−dimer equilibrium. In future studies, this hypothesis will be tested by analytical ultracentrifugation studies of the monomer−dimer equilibrium as a function of salt concentration at neutral pH.

CAR-D1 Protein−Protein Interactions. Finally, it is of interest to consider the importance of the CAR-D1 monomer−dimer equilibrium to its role in cell adhesion, as well as its role in viral entry. Based on the X-ray structure of the CAR-D1 dimer (*14*), the self-interaction surface is shown in Figure 7a in cyan. The self-interaction face consists of many of the residues discussed above (e.g., the exposed hydrophobic side chains of L58, V67, V70, L73, and V128 and the charged side chains of D54, E56, and K123). The CAR-D1/Ad interaction surface is shown in Figure 7a in red, based on the X-ray structure of CAR-D1 bound to the Ad fiber head (*15*). Again, many of the same residues are involved in the intermolecular interaction and, as previously noted (*14*), the interaction sites largely overlap consistent with the notion that Ad binds to monomeric CAR-D1. Furthermore, the cryoelectron microscopy structure of CAR-D1/D2 bound to CVB also demonstrates that CVB binds to the monomeric state of CAR-D1 (*16*). The putative CVB interaction site of

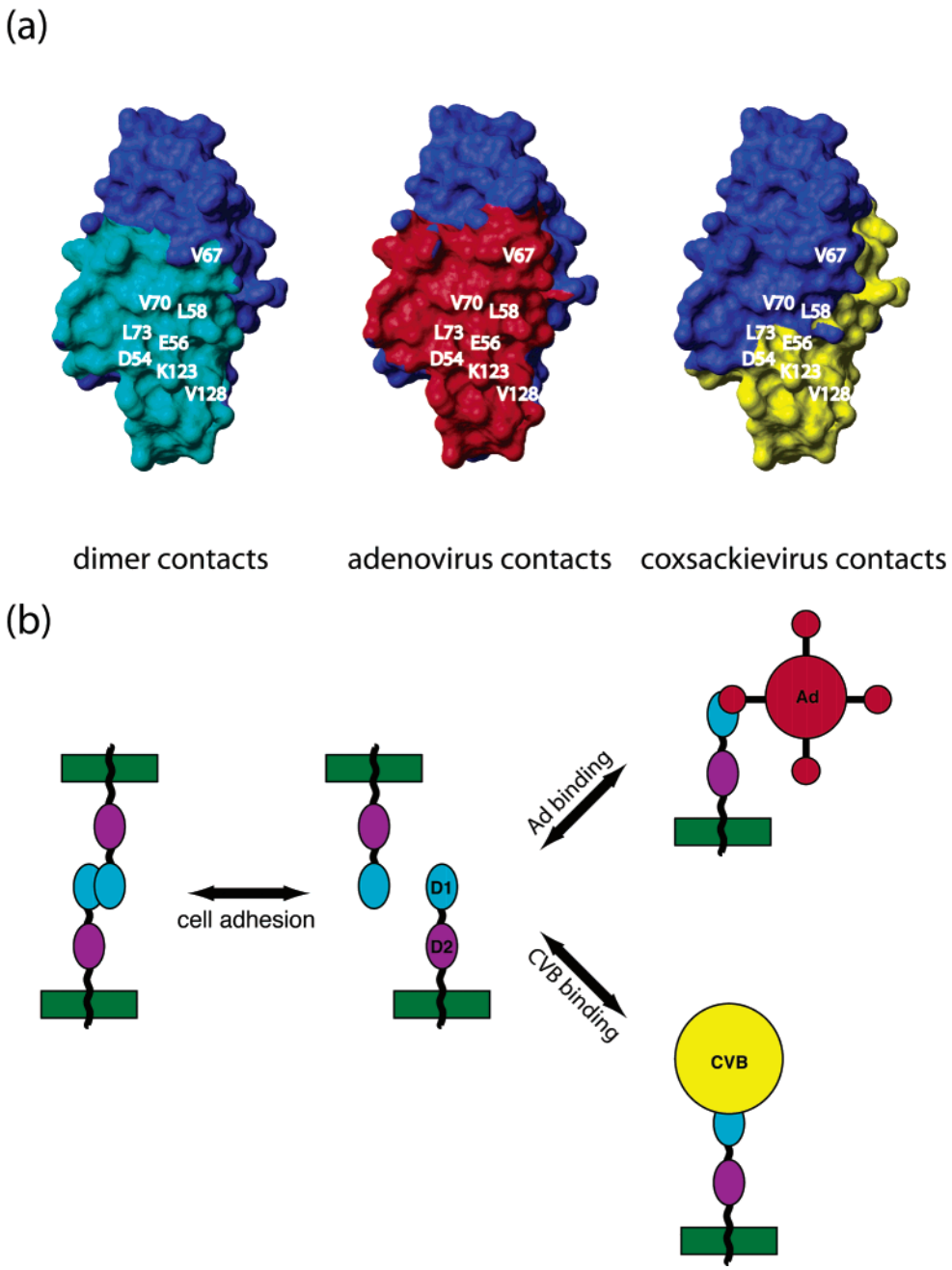

FIGURE 7: Analysis (a) of the binding sites on CAR-D1. The dimeric contacts observed in the X-ray structure of CAR-D1 at pH 5.2 are shown in cyan (*14*). The Ad contacts observed in the X-ray structure of CAR-D1/adenovirus fiber head at pH 6.2 are shown in red (*15*). The CVB contacts observed in the cryoelectron microscopy structure of CAR-D1D2/CVB are shown in yellow (*16*). Panel b shows a schematic representation of CAR-D1 intermolecular interactions based on the structures of the monomer (present work), dimer (*14*), complex with the Ad fiber head (*15*), and complex with CVB (*16*).

CAR-D1 is shown in Figure 7a in yellow. Interestingly, as previously noted (*16*), the CVB interaction site only partially overlaps with the self-association and Ad sites. Nonetheless, the charged side chains D54, E56, and K123 and the exposed hydrophobic side chains L73 and V128 are apparently also involved in the CAR-D1/CVB interaction. Taken together, these observations are consistent with the model presented in Figure 7b. In this model, the normal physiological function of CAR is involvement in cell adhesion. In this role, the CAR-D1 domains form an antiparallel dimer with the CAR-D1 of neighboring cells, consistent with the X-ray structure of the CAR-D1 dimer (*14*) and similar to the case for other proteins involved in neuronal cell adhesion (reviewed in ref *37*). The self-association in vitro has a K_d of 16 μM, and thus, it is reasonable to hypothesize that in vivo the self-association is relatively weak with an equilibrium between the monomer and dimer states as shown in Figure 7b. The viruses Ad and CVB have evolved to bind to the monomeric state of CAR-D1. Interestingly, viral binding is favored by a much stronger association to the CAR-D1 monomer (e.g., the K_d for CAR-D1 binding to the Ad fiber head is $\sim$20 nM, *38*), similar to the case of numerous other interactions between viruses and receptors (reviewed in ref *39*). Our long-term goal is to develop NMR-based drug discovery against Ad and CVB binding to CAR, and consequently, the monomer structure of CAR-D1 determined in the present

work will serve as a model system for future studies of viral association with CAR.

ACKNOWLEDGMENT

Professor Bergelson is gratefully acknowledged for providing a clone of the CAR DNA.

SUPPORTING INFORMATION AVAILABLE

Table S1, which contains the relaxation data (R_z, R_{xy}, and HNOE) and the derived relaxation parameters (S^2, τ_e, R_{ex}, and Sf^2) for CAR-D1. This material is available free of charge via the Internet at http://pubs.acs.org.

REFERENCES

1. Pallansch, M. (1997) Coxsackievirus B epidemiology and public health concerns, *Curr. Top. Microbiol. Immunol. 223*, 13−30.
2. Modlin, J., and Rotbart, H. (1997) Group B Coxsackie disease in children, *Curr. Top. Microbiol. Immunol. 223*, 54−74.
3. Abelmann, W. H. (1973) Viral myocarditis and its sequelae, *Annu. Rev. Med. 24*, 145−152.
4. Lau, R. C. (1983) Coxsackie B virus infections in New Zealand patients with cardiac and noncardiac diseases, *J. Med. Virol. 11*, 131−137.
5. Ellis, R. W. (1997) Infection and coronary heart disease, *J. Med. Microbiol. 46*, 535−539.
6. Baboonian, C., Davies, M., Booth, J., and McKenna, W. (1997) Coxsackie B virus and human heart disease, *Curr. Top. Microbiol. Immunol. 223*, 31−53.
7. Bergelson, J., Cunningham, J., Droguett, G., Durt-Jones, E., Drithaivas, A., Hong, J., Horwitz, M., Crowell, R., and Finberg, R. (1997) Isolation of a common receptor for Coxsackie B viruses and Adenoviruses 2 and 5, *Science 275*, 1320−1323.
8. Tomoko, R., Xu, R., and Philipson, L. (1997) HCAR and MCAR: the human and mouse cellular receptors for subgroup C adenoviruses and group B coxsackieviruses, *Proc. Natl. Acad. Sci. U.S.A. 94*, 3352−3356.
9. Carson, S., Chapman, N., and Tracy, S. (1997) Purification of the putative coxsackievirus B receptor from HeLa cells, *Biochem. Biophys. Res. Commun. 233*, 325−328.
10. Kuhn, R. (1997) Identification and biology of cellular receptors for the coxsackie B viruses group, *Curr. Top. Microbiol. Immunol. 223*, 209−226.
11. Honda, T., and Kuwano, R. (2000) The coxsackievirus-adenovirus receptor protein as a cell adhesion molecule in the developing mouse brain, *Brain Res. Mol. Brain Res. 14*, 19−28.
12. Wang, X., and Bergelson, J. (1999) Coxsackievirus and adenovirus receptor cytoplasmic and transmembrane domains are not essential for coxsackievirus and adenovirus infection, *J. Virol. 73*, 2559−2562.
13. Leon, R. P., Hedlund, T., Meech, S. J., Li, S. B., Schaack, J., Hunger, S. P., Duke, R. C., and DeGregori, J. (1998) Adenoviral-mediated gene transfer in lymphocyte, *Proc. Natl. Acad. Sci. U.S.A. 95*, 13159−13164.
14. Van Raaij, M., Chouin, E., van der Zandt, H., Bergelson, J., and Cusack, S. (2000) Dimeric structure of the coxsackievirus and adenovirus receptor D1 domain at 1.7 Å resolution, *Structure 8*, 1147−1155.
15. Bewley, M., Springer, K., Zhang, Y.-B., Freimuth, P., and Flanagan, J. (1999) Structural analysis of the mechanism of adenovirus binding to its human cellular receptor, CAR, *Science 286*, 1579−1583.
16. He, Y., Chipman, P., Howitt, J., Bator, C., Whitt, M., Baker, T., Kuhn, R., Anderson, C., Freimuth, P., and Rossman, M. (2001) Interaction of cosackievirus B3 with the full length coxsackievirus-adenovirus receptor, *Nat. Struct. Biol. 8*, 874−878.
17. Jiang, S., and Caffrey, M. (2002) Assignment of the ^{1}H, ^{13}C and ^{15}N resonances of the coxsackievirus and adenovirus receptor domain 1, *J. Biomol. NMR 24*, 365−366.
18. Stafford, W. (1992) Boundary analysis in sedimentation transport experiments: a procedure for obtaining sedimentation coefficient distributions using the time derivative of the concentration profile, *Anal. Biochem. 203*, 295−301.
19. Philo, J. (2000) A method for directly fitting the time derivative of sedimentation velocity data and an alternative for calculating sedimentation coefficient distribution functions, *Anal. Biochem. 279*, 151−163.
20. Brunger, A., Adams, P., Clore, G., DeLano, W., Gros, P., Grosse-Kunstleve, R., Jiang, J.-S., Kuszewski, J., Nilges, N., Pannu, N., Read, R., Rice, L., Simonson, T., and Warren, G. (1998). Crystallography and NMR system (CNS): A new software system for macromolecular structure determination, *Acta Crystallogr. D54*, 905−921.
21. Guilhaudis, L., Jacobs, A., and Caffrey, M. (2002) Solution structure of the HIV gp120 C5 domain, *Eur. J. Biochem. 269*, 4860−4867.
22. Cornilescu, G., Delaglio, F., and Bax, A. (1999) Protein backbone angle restraints from searching a database for chemical shift and sequence homology, *J. Biomol. NMR 13*, 289−302.
23. Koradi, R., Billeter, M., and Wuthrich, K. (1996) MOLMOL: a program for display and analysis of macromolecular structures, *J. Mol. Graphics 14*, 52−55.
24. Cavanagh, J., Fairbrother, W., Palmer, A., and Skelton, N. (1996) *Protein NMR Spectroscopy*, Academic Press, San Diego.
25. Nicholson, L., Kay, L., Baldisseri, D., Arango, J., Young, P., Bax, A., and Torchia, D. (1992) Dynamics of methyl groups in proteins as studied by proton-detected ^{13}C NMR spectroscopy, application to the leucine residues of Staphylococcal nuclease, *Biochemistry 31*, 5253−5263.
26. Dosset, P., Hus, J., Blackledge, M., and Marion, D. (2000) Efficient analysis of macromolecular rotational diffusion from heteronuclear relaxation data, *J. Biomol. NMR 16*, 23−28.
27. Lipari, G., and Szabo, A. (1982) Model-free approach to the interpretation of nuclear magnetic resonance relaxation in macromolecules. 1. Theory and range of validity, *J. Am. Chem. Soc. 104*, 4546−4559.
28. Laue, T. (2001) Biophysical studies by ultracentrifugation. *Curr. Opin. Struct. Biol. 11*, 579−583.
29. Laskowski, R., MacArthur, M., Moss, D., and Thorton, J. (1993) PROCHECK − a program to check the stereochemical quality of protein structures, *J. Appl. Crystallogr. 26*, 283−291.
30. Ruckert, M., and Otting, G. (2000) Alignment of biological macromolecules in novel nonionic liquid crystalline media for NMR experiments, *J. Am. Chem. Soc. 122*, 7793−7797.
31. Wishart, D., and Case, D. (2001) Use of chemical shifts in macromolecular structure determination, in *Methods in Enzymology*, (James, Dotsch, and Schmitz, Eds.) Vol. 338, Academic Press, New York.
32. Young, L., Jernigan, R., and Covell, D. (1994) A role for surface hydrophobicity in protein−protein interactions, *Protein Sci. 3*, 717−729.
33. Jones, S., and Thorton, J. (1996) Principles of protein−protein interactions, *Proc. Natl. Acad. Sci. U.S.A. 93*, 13−20.
34. Palmer, A. (1997) Probing molecular motions by NMR, *Curr. Opin. Struct. Biol. 7*, 732−737.
35. Kay, L. (1998) Protein dynamics from NMR, *Nat. Struct. Biol. 5*, 513−517.
36. Barlow, D., and Thornton, J. (1983) Ion-pairs in proteins, *J. Mol. Biol. 168*, 867−885.
37. Kiss, J., Troncoso, E, Djebbara, Z., Vutskits, L., and Muller, D. The role of neural cell adhesion molecules in plasticity and repair, *Brain Res. Rev. 36*, 175−184.
38. Lortat-Jacob, H., Chouin, E., Cusack, S., and van Raaij, M. (2001) Kinetic analysis of adenovirus fiber binding to its receptor reveals an avidity mechanism for trimeric receptor−ligand interactions, *J. Biol. Chem. 276*, 9009−9015.
39. Wang, J.-H. (2002) Protein recognition by cell surface receptors: physiologic receptors versus virus interactions, *Trends Biochem. Sci. 27*, 122−126.

BI035490X